

## Supplemental Materials

A population framework for predicting the proportion of people infected by the far-field airborne transmission of SARS-CoV-2 indoors

Christopher Iddon<sup>a</sup>, Benjamin Jones<sup>a,\*</sup>, Patrick Sharpe<sup>a</sup>, Muge Cevik<sup>b</sup>,  
Shaun Fitzgerald<sup>c</sup>

<sup>a</sup>*Department of Architecture and Built Environment, University of Nottingham,  
Nottingham, UK*

<sup>b</sup>*Infection and Global Health Division, School of Medicine, University of St Andrews, St  
Andrews, UK*

<sup>c</sup>*Department of Engineering, Cambridge University, Cambridge, UK*

---

*Keywords:* relative exposure index, airborne, ventilation, aerosols,  
transmission risk, viral load, COVID-19,

---

---

\*Corresponding author

*Email address:* benjamin.jones@nottingham.ac.uk (Benjamin Jones)

*Preprint submitted to .*

*November 24, 2021*

## 1. Model uncertainties

The output of the REI is a dose value of RNA copies that deposit onto the respiratory tract of a susceptible individual (for brevity we will term this the inhaled dose). The number of viral genome copies (RNA copies) is proportional to the number of viable virion, but the ratio of RNA copies to viable virion is unknown. Whether the deposited virion then leads to an infection in the susceptible individual depends upon the dose response – another unknown quantity, and the susceptibility of the individual to infection.

### 1.1. Uncertainty in dose response

There is currently no dose–response curve for SARS-CoV-2, however a number of studies have used a proposed dose curve for SARS-CoV-1, which is a typical coronavirus dose curve [1, 2, 3]. This dose curve was generated from inoculating four groups of transgenic mice (mice genetically modified to express the the human protein that is the receptor for the SARS-CoV-1 virus). The dose response curve was fitted to data from these four groups, in three of which all of the mice became infected and in one group a third of mice become infected. This is a limited data set for curve fitting, although it is sufficient to assume that the dose curve is exponential rather than a Beta-Poisson distribution. It should be noted that the dose response of humans may vary significantly from that of transgenic mice.

Dose curves are fitted to low PFU but there is usually limited data at very low doses. Therefore, the dose-response relationship is highly uncertain at low doses and infection probabilities. This is important because, when considering a large population, even very low probabilities of infection could

25 lead to a significant number of infected people – and it may well be an  
26 overestimation if the dose-response curve at very low level of virus is not  
27 representative.

28 In another study Schijven *et al.* determined a model that 1440 RNA copies  
29 was required to lead to an infection, drawing assumptions from the proportion  
30 of isolated cultured SARS-CoV-2 (ie not collected from patient swabs) needed  
31 to infect a cell culture line to calculate a PFU and then deriving an infectious  
32 dose from a dose curve for human coronavirus 229E of 1,440 RNA copies  
33 [4]. Uncertainties are that SARS-CoV-2 isolate unlikely to be comparable  
34 to SARS-CoV-2 collected from patient samples eg swabs. The response of  
35 a cell culture is unlikely to be comparable to a respiratory tract, mucosal  
36 membranes and innate immunity of a human. The dose curve for 229E may  
37 also be different to that for SARS-CoV-2.

38 There are challenges and uncertainties in the assumptions used to gener-  
39 ate infective dose-response curves for SARS-CoV-2 and as these uncertainties  
40 are not easily measurable, there will be unknown uncertainties in calculating  
41 the probability of infection using such assumptions.

#### 42 *1.2. Uncertainty in viral load*

43 It has been well established that the viral load of an infector increases from  
44 the date of infection and is highest just before or at the onset of symptoms,  
45 and as the disease progresses the viral load begins to reduce (within the  
46 first week of symptom onset) [5, 6]. Viral load at any stage of infection  
47 also varies between individuals, which increases the uncertainty in this value  
48 [7, 8, 9, 10, 11, 12]. Some studies use reported cycle threshold values from  
49 real time reverse transcription quantitative polymerase chain reaction (RT

50 qPCR) nasopharyngeal (NP) swabs to infer the viral load in respiratory fluid,  
51 however this method assumes a direct correlation between the swab viral load  
52 and the respiratory fluid viral load [13, 14]. RT qPCR is semi-quantitative  
53 in that the number of cycles required to provide a positive signal for SARS-  
54 CoV-2 genome is proportional to the starting amount of viral genome in  
55 the sample. The greater the number of amplification cycles required, the  
56 lower the starting amount of viral genome. A calibrated standard curve  
57 can then be used to estimate the starting amount of viral genomic material.  
58 However, the standard curve varies between test assays and different RT  
59 qPCR thermal cyclers. This method assumes a complete doubling of genetic  
60 material at each cycle, and because of the logarithmic relationship, the errors  
61 in calculating the starting genomic material for low cycle counts are orders  
62 of magnitude higher than those with high cycle counts. Additionally, the  
63 estimated concentration of genomic material per unit volume is related to  
64 the amount of genomic material in the buffer solution used in the assay,  
65 not necessarily the amount in the patients respiratory fluid if data is from  
66 NP swabs. The amount of genomic material added to the buffer solution is  
67 dependent on not only the viral load of the patient, but also the quality of  
68 NP sample collection, which is highly variable. Therefore, it is not possible  
69 to determine absolute values of the viral load in patient’s respiratory fluid  
70 using this method, although it is indicative of a range of variability – much  
71 of which is likely to be proportional to the viral load of the individual at  
72 the time the sample was collected. While it is somewhat correlated, recent  
73 data suggests that the viral load of NP swabs may not reflect the amount  
74 of infectious material present [10]. However, it is important to note that

75 there are wide variations in the measured genomic material in NP swabs  
76 and that viral load in respiratory fluid is likely to vary over several orders of  
77 magnitude, although absolute values and proportions are not determinable  
78 with current data.

79 The RT-qPCR process also only amplifies a small section of viral genome  
80 and is representative of viral genomic material in the original sample. Some of  
81 this genomic material will be fragments, and therefore quantities of genomic  
82 material are not representative of the number of viable virions in the original  
83 sample, although likely to be proportional to, and there is some evidence  
84 in the literature to suggest there is some correlation between Ct values and  
85 infectious virus [6]. Additionally, one study of the influenza virus showed  
86 that the viral load in NP swabs was not a significant predictor of aerosol  
87 shedding [15]. In other studies the SARS-CoV-2 viral load of saliva has been  
88 estimated using qRT-PCR that also show wide variability of several orders  
89 of magnitude, although it is unknown if the saliva viral load is the same as  
90 the viral concentration in the fluid of the respiratory tract[16].

### 91 *1.2.1. Viral load in aerosols*

92 If the viral load in respiratory fluid could be determined it is currently  
93 unclear whether the viral concentration in respiratory aerosols and droplets  
94 is uniformly distributed. Some studies suggest that the amount of virion in  
95 smaller aerosols ( $< 1 \mu\text{m}$ ) is higher than would be expected given the viral  
96 concentration in the respiratory fluid [17, 18] and that there may be more  
97 genomic material in the smallest aerosols [19]. There is also high variability  
98 in the total volume of aerosols generated per unit volume of exhaled breath  
99 between individuals, which is especially true for breathing and is dependent

100 upon the respiratory activity and respiratory capacity (e.g. talking, singing)  
101 [20, 21, 22, 23]. A recent study from Coleman *et al.* [19] has detected SARS-  
102 CoV-2 genomic material in expired aerosols from *some* Covid patients,  
103 although 41% percent of patients exhaled no detectable genomic material.  
104 Singing and talking generally produced more genomic material than breath-  
105 ing, but there was large variability between patients. This suggests that res-  
106 piratory activities that have previously been shown to increase aerosol mass,  
107 also increase the amount of viral genomic material, although in this study  
108 the viral concentration in aerosols cannot be determined because the mass  
109 of aerosols generated was not measured. It also shows that the variability in  
110 the amount of genomic material measured in expired aerosols is consistent  
111 with the variability of viral loads as measured by swabs and saliva [19]. Sim-  
112 ilarly Adenaiye *et al.* have also detected genomic material in aerosols from  
113 patients infected with SARS-CoV-2 providing a sampled of exhaled air with  
114 some talking and singing. Genomic material was most likely to be detected in  
115 exhaled aerosols when the viral load of saliva or Mid-turbinate swabs (MTS)  
116 was high ( $> 10^8 RNA\ copies$  and  $> 10^6$  for MTS and saliva samples respec-  
117 tively). Additionally they were also able to culture viable virus from  $< 2\%$   
118 of fine aerosol samples (although one culture positive sample was from a fine  
119 aerosol sample which has a less than Limit Of Detection amount of genomic  
120 material as measured by RT-PCR, so could be an artefact). Providing some  
121 evidence to support the epidemiological evidence that viable virus can exist  
122 in exhaled aerosols [24].

123 Buonanno *et al.*, although noting that there are no values available in the  
124 literature, propose a method to convert viral load to quanta emission rate

125 (where a quantum is defined as the dose of airborne droplet nuclei required to  
126 cause infection in 63% of susceptible people) using a value for PFU per quanta  
127 derived from Watanabe *et al.*, see Section 1.1, and RNA copies per PFU from  
128 Fear *et al.* - values derived from stock SARS-CoV-2 created from Vero E6  
129 cells, values which may well not reflect the quanta emission rate in an infected  
130 person [25, 1, 26]. There is likely much uncertainty in this method and how  
131 representative it is of infector viral emission rates.

### 132 1.3. Estimating viral emission from viral load

133 Although we have a range of viral loads for infectors in RNA copies per  
134 ml, estimating how that relates to the emission of rna per unit time is  
135 challenging due to the uncertainties listed, however, if we assume that the  
136 RNA copies concentration is constant in aerosols and NP swabs we can use  
137 the assumptions of Jones *et al.* [27] to convert a NP viral load into a viral  
138 shedding rate. This methodology is derived from the aerosol volume distri-  
139 bution of different respiratory activities from Morawskwa *et al.* and is similar  
140 to that used by Lelieveld *et al.* [28, 23]. Table 1 shows that for a viral load of  
141  $10^7$  RNA copies per ml this would assume the RNA copies shedding per hour,  
142 and for comparison median values from Coleman *et al.* study are given, in  
143 which the measured collected RNA copies were from Covid patients with a  
144 median Ct of 16 from the patient's diagnostic sample [19].

145

Table 1: Estimated RNA copies shedding rates from an infector with a viral load of  $10^7$  RNA copies per ml compared to measured RNA copies shedding rates from patients with a median Ct of 16 as measured by Coleman *et al.* \*value calculated from breathing and talking values

	estimated	measured median
	$RNA\ copies\ h^{-1}$	$RNA\ copies\ h^{-1}$
Breathing	203	127
Voiced counting (talking)	967	1912
Vocalisation (singing)	6198	2856
Breathing:talking 25:75	394	573*

146 Additionally a recent pre-print from Adenaiye *et al.* has also measured  
 147 viral genome in patients, infected with SARS-CoV-2 alpha variant, breath-  
 148 ing with some talking in coarse ( $5\mu m$ ) and fine ( $\leq 5\mu m$ ) aerosols with a  
 149 total geometric mean of 1440  $RNA\ copies\ h^{-1}$  (with a maximum of  $3 \times 10^5$   
 150  $RNA\ copies\ h^{-1}$ ) [24]. Although this is more than the estimated values in  
 151 Table 1, the viral load as measured by genome copies from Mid-turbinate  
 152 swabs (MTS) was generally orders of magnitude higher than  $10^7$ .

153 In the measured data we don't know the relationship between the PCR  
 154 cycle threshold and the patient viral load in  $RNA\ copies/ml$ , however the cal-  
 155 culated shedding rate of viral genome for a viral load of  $10^7$  RNA copies per ml  
 156 is a reasonable fit to the Coleman *et al.* and Adenaiye *et al.* data.

157 Other studies have suggested that genome emission rates of patients could  
 158 be of the order of  $10^6\ RNA\ copies\ h^{-1}$ . Miller *et al.* derived this value from  
 159 RNA copies measured in small hospital rooms containing Covid patients (here  
 160 the air sampling equipment is located quite close to the patient and some  
 161 observation that patients face turned to face collector for some samples) [29,



162 14]. Whilst Ma *et al.* collected viral genome in exhaled breath of patients that  
163 would suggest patients exhaled in the region of  $7 \times 10^4$  to  $7 \times 10^6$  RNA copies per  
164 hour, though in this study the collection mechanism involved exhaling into a  
165 small straw-like tube for 5 minutes, which could also become contaminated  
166 with viral laden saliva, thus over estimating the viral load of the exhaled  
167 breath [30]. Although these exhaled rates of viral genome are much greater  
168 than those collected by Coleman *et al.*, Miller *et al.* notes that suggests that  
169 around 1 : 1000 genome copies are likely to be infectious virion [31, 14].  
170 Adenaiye *et al.* suggest that from MTS there is around 1 :  $10^4$  viable virus  
171 per measured genome copies[24]. For this study we have made the assumption  
172 that all genome copies are viable virion, which either over-estimates the likely  
173 infectiousness if using the Coleman *et al.* data, or is similar to the Miller *et*  
174 *al.* assumptions if the viable virion shedding rate is in the order of 1000  
175 virion per hour.

176 For the proportion of persons infected analysis, the inhaled dose is calcu-  
177 lated for all viral loads, it should be noted that the calculated RNA copies  
178 shedding rate is assumed to scale linearly with viral load per ml of respi-  
179 ratory fluids, such that a viral load of  $10^8 \text{ RNA copies/ml}$  would have ten  
180 fold greater RNA copies shedding rates per hour. For comparison, given  
181 a viral shedding of 394 RNA copies per hour (assumed for a viral load of  
182  $10^7 \text{ RNA copies/ml}$ ) would lead to an individual inhaled dose of around 2.2  
183 and 0.2 RNA copies for the Small Office and Big Office scenarios respectively.

### 184 1.3.1. Comparison of viral emission from literature

185 Extrapolating data for viral shedding rates from the literature is challeng-  
186 ing as often the estimated doses and the probability of infection do not align

187 with epidemiological evidence. Chen *et al.* suggests that the upper limit for  
188 the total virion shedding rate for moderate talking is 6000 virions per hour.  
189 This includes droplets up to  $100\ \mu\text{m}$  and so we assume the evaporation and  
190 suspension of all these droplets in the air, although it is unlikely. Given a  
191  $600\ \text{m}^3$  20 person office at  $10\ \text{l s}^{-1}$  per person with an infected person shed-  
192 ding at 100 virions per minute we would expect  $< 10$  virions to deposit in the  
193 respiratory tract of a susceptible person over an 8 hour day, which, from the  
194 DeDiego *et al.* SARS-CoV-1 dose curve, is unlikely to lead to an infection.  
195 This suggests that if the upper limit of viral shedding is unlikely to result  
196 in an infection, than the more likely lower viral shedding rates will be even  
197 more unlikely to give rise to infection [32, 12].

198 Using the shedding rate of 6000 virions per hour for the Skagit choir  
199 (Miller *et al.* [14] suggest shedding at 1000 virions per hour would be a rea-  
200 sonable estimate for this scenario) we expect a susceptible person to have  
201 about 7 virions deposit in their respiratory tract over a 2.5 hour practice pe-  
202 riod. Using the SARS-CoV-1 dose curve, this gives a probability of infection  
203 of 0.02. Given that the secondary attack rate at the Skagit choir was over  
204 85%, this would suggest that either the  $k$  value in the SARS-CoV-2 dose  
205 curve (see Equation 2) is much smaller than that predicted for SARS-CoV-1  
206 or these models have used assumptions that have under estimated the virion  
207 shedding rate, even for the high viral emitter considered here.

208 Alternatively, the quanta metric could be used because it captures the  
209 effects of virion shedding and the dose curve by associating secondary trans-  
210 mission in a particular transmission event. The quanta for the Skagit event  
211 is calculated by Miller *et al.*, where the dose is likely to be  $1.19 \pm 0.48$  quanta.

212 Using the Wells-Riley model gives a probability of transmission of between  
213 0.51 and 0.81. This suggests that the quanta method is a better fit in this  
214 Skagit choir scenario, although this is to be expected because the quanta  
215 emission rate is exclusively derived from the number of secondary transmis-  
216 sion events that occurred during the scenario.

217 If we use the Skagit quanta emission rate in another scenario, say a UK  
218 junior school classroom described by Jones *et al.* [27], then it is possible to  
219 conclude the following: the emission rate for singing is  $970 \pm 390 \text{ q h}^{-1}$  but  
220 assume a 30-fold reduction for aerosol emission when breathing and assume  
221 a child breath rate ( $q_{sus}$ ) of  $0.44 \text{ m}^3 \text{ h}^{-1}$ , then the dose over a 7 hour exposure  
222 period is  $0.77 \pm 0.31$  quanta, giving a probability of infection between 0.37 and  
223 0.66. Although transmission events do occur in school classrooms, there isn't  
224 evidence to suggest such high rates of secondary far-field transmission occur  
225 regularly. Secondary attack rates (for all routes of transmission) amongst  
226 primary pupils have been recorded at less than 1% [33] (although more recent  
227 observations on infection rates amongst UK school age children in Autumn  
228 2021 suggests secondary attack rates are likely to be higher than this for the  
229 Delta variant, however, still not at probability of infection between 0.37 and  
230 0.66 [34]). This suggests that the quanta emission rate (as estimated in the  
231 Skagit Choir scenario) is either extremely unlikely or it scenario-specific and  
232 so it is inappropriate to use a quanta emission rate determined from a single  
233 scenario and apply to another.

234 **2. Results and discussion: Effect of varying model assumptions on**  
 235 ***PPI***

236 In addition to the results reported in the main paper, here we report  
 237 the effect of various model assumptions on the *PPI* and *TR*. All standard  
 238 scenario inputs are given in Tables 2 and 3.

Table 2: Scenario inputs and calculations of individual risk.

	Big Office Reference	Small Office Comparator
Number of occupants, $N$	50	5
Space Volume, $V$ ( $\text{m}^3$ )	1500	150
<i>Per capita</i> volume, $V N^{-1}$ ( $\text{m}^3$ per person)	30	30
Air flow rate, $\psi V$ ( $\text{ls}^{-1}$ )	500	50
Air change rate, $\psi$ ( $\text{h}^{-1}$ )		1.2
Removal rate, $\phi$ ( $\text{h}^{-1}$ )	2.26	2.26
Equivalent ventilation rate, $\phi V$ ( $\text{ls}^{-1}$ )	942	94.2
Exposure time, $T$ (h)	8	8
Dose constant, $k$ [32]	410	410
Viable fraction, $v$ (%)	100	100
Viral load (RNA copies per ml) [35]	$10^7$	$10^7$
Respiratory activity, <i>breathing: talking</i> (%)	75:25	75:25
Viral emission rate, $G$ (RNA copies per hour)	394	394
Respiratory rate, $q_{sus}$ ( $\text{m}^3\text{h}^{-1}$ )	0.56	0.56
Community infection rate, $C$	1:100	1:100
Dose, $D$ (viable virions inhaled)	0.245	2.450
REI	1	10

All values converted to SI units before application.

239 *2.1. Dose curve constant  $k$*

240 Figure 1 shows that when the dose  $k$  values are low ( $< 50$ ) then the *PPI*  
 241 begins to increase rapidly as lower doses are required to result in a significant  
 242 proportion of susceptibles in a scenario population becoming infected. The

Table 3: Scenario inputs and calculations of population risk.

	Big Office Reference	Small Office Comparator
Viral load [35] (RNA copies per ml)	LN( $2.1 \times 10^9, 2.0 \times 10^{10}$ )	
$P(R)$ (%)	0.062	0.620
$P(I = 0)$ (%)	61	95
$P(0 < I < N)$ (%)	39	5
$\bar{I}$	1.27	1.02
$P(S)$ (%)	39	5
$PPI$ (%)	1.59	0.43
$TR$		0.27

LN, log-normal( $\mu, \sigma$ )  
All values converted to SI units before application.

243 rate of increase in  $PPI$  is greater in Big Office due to the larger population of  
244 susceptibles. This results demonstrate that the dynamics of the dose response  
245 are important in understanding the  $PPI$  and more work is required to better  
246 understand these characteristics for SARS-CoV-2. Epidemiological evidence  
247 can provide some illumination as to what bounds values of  $k$  with respect to  
248 measured far-field transmission rates in indoor scenarios.

## 249 2.2. Virion viability

250 In our study, we take the conservative assumption that all viral genome  
251 copies (RNA copies) in an inhaled dose are viable virions. The actual pro-  
252 portion it more likely to be orders of magnitude lower, with estimates in the  
253 literature of a range of 1 : 100 to 1 : 10000 of viable virions to RNA copies.  
254 Miller *et al.* suggests that around 1 : 1000 genome copies are likely to be in-  
255fectious virion whilst Adenaiye *et al.* suggest that from mid-turbinate swabs  
256 there is around 1 :  $10^4$  viable virus per measured genome copies[14, 24].

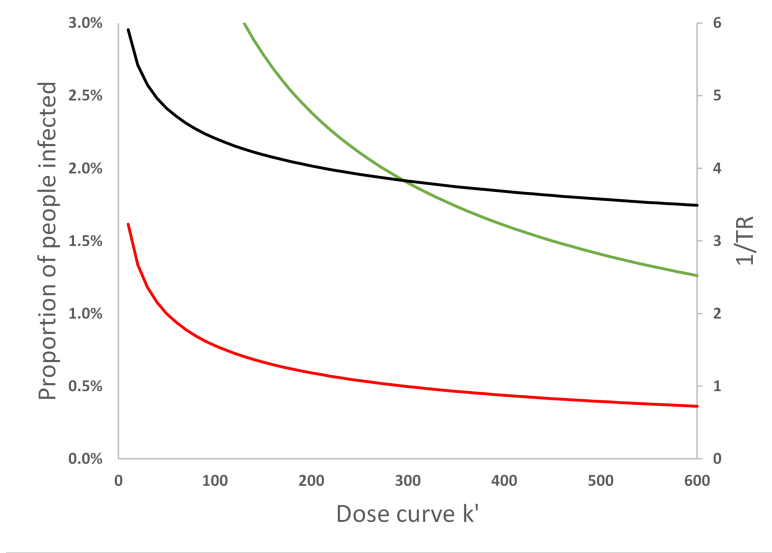


Figure 1: The effect of increasing the dose curve constant,  $k$ , on the Big Office  $PPI$  (green), Small Office  $PPI$  (red) and the  $TR$  (black). As  $k$  increases the size of the inhaled dose needed to give an equivalent probability of infection increases. All values are illustrative.

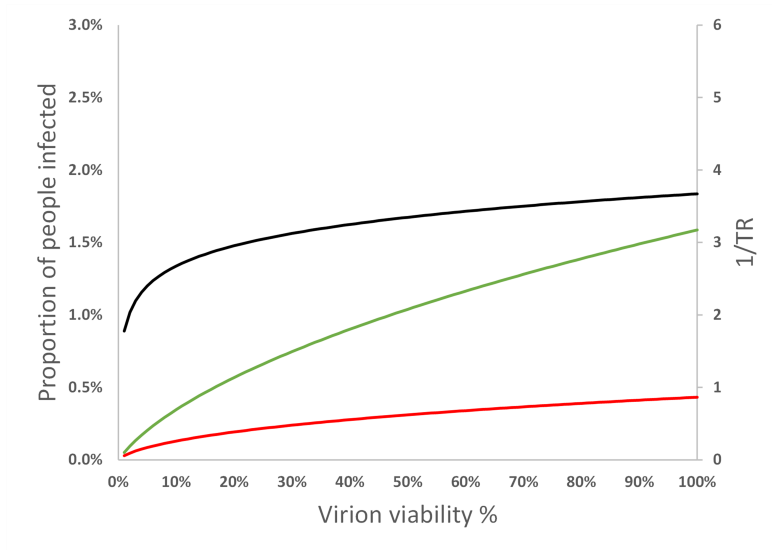


Figure 2: The effect of increasing the virion viability on the Big Office  $PPI$  (green), Small Office  $PPI$  (red) and the  $TR$  (black). As the proportion of RNA copies in the inhaled dose that are viable of virions increase, the probability of infection increases. All values are illustrative.

257 Figure 2 shows the  $PPI$  in both Big Office and Small Office reduces as  
 258 the proportion of viable virions decreases. Whilst the  $TR$  decreases, the  
 259 ratio of Small Office to Big Office remains above 2, but the absolute values  
 260 of  $PPI$  become very low as virion viability  $< 1\%$ , suggesting that far-field  
 261 transmission, given the assumptions in Tables 2 and 3, is very unlikely if  
 262 virion viability is low.

263 *2.3. Viral Load of infected*

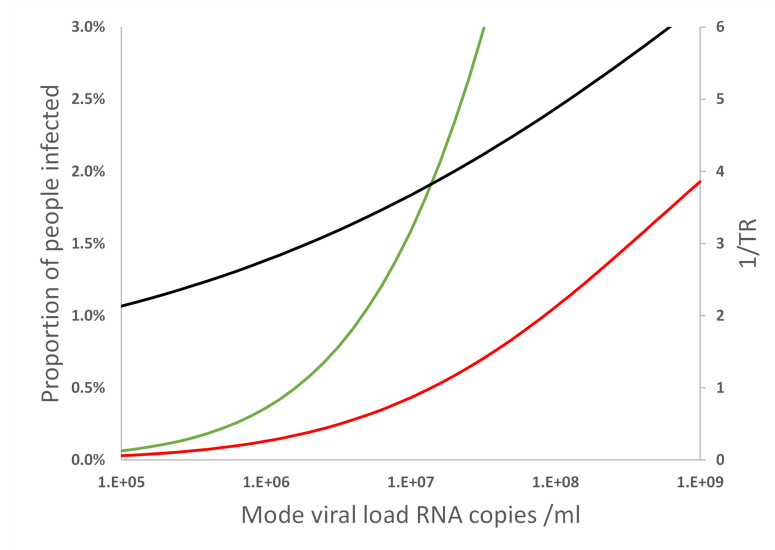


Figure 3: The effect of increasing the mode viral load of the infected population on the Big Office  $PPI$  (green), Small Office  $PPI$  (red) and the  $TR$  (black). As the mode viral load of the infectors increases, the emission rate of RNA copies increases, resulting in an increase in dose and  $PPI$ . All values are illustrative.

264 The inhaled dose is also a function of the viral load distribution within  
 265 the infected population. We assume that it is log normally distributed with  
 266 a mean of  $\mu = 2.1 \times 10^9$  and a standard deviation of  $\sigma = 2.0 \times 10^{10}$ . Figure 3  
 267 shows the change in the probability of transmission and the  $TR$  when the

268 mean log value of the distribution is varied between 5 and 9. When the mean  
 269 is low, the probability of one or more infectors having a sufficiently high  
 270 emission rate to lead to the inhalation of an infective dose is very low, ie when  
 271  $\mu = 5$ . Conversely, increasing the probability of the infectors having a high  
 272 viral load (by increasing  $\mu$ ) rapidly increases the probability of transmission  
 273 in both scenarios, and an increase in the  $TR$ .

274 *2.4. Space Volume per person*

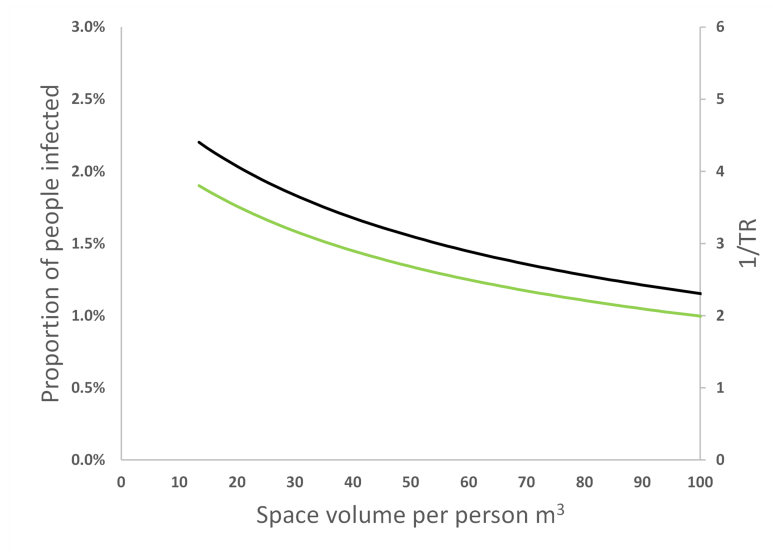


Figure 4: The effect of increasing the *per capita* space volume,  $V$ , in the Big Office on the  $PPI$  (green) and the  $TR$  (black) when the *per capita* space volume in the Small Office is constant. All values are illustrative.

275 Figure 4 shows that increasing the *per capita* space volume in the Big  
 276 Office when the *per capita* space volume in the Small Office, while maintain-  
 277 ing a constant *per capita* ventilation in both spaces has a similar effect to  
 278 increasing the *per capita* ventilation. This is because the dose is inversely  
 279 proportional to volume. Furthermore, the product of the space volume and



280 the total removal rate,  $\phi V$ , is proportional to the concentration of the virus  
281 in the air and, therefore, the dose. The *per capita* ventilation rate is constant  
282 in both spaces and so the air change rate in the Big Office decreases as its  
283 volume increases. However, this reduction is offset by the surface deposition  
284 and biological decay rates, which remain constant and have a greater effect  
285 on the value of the equivalent ventilation rate,  $\psi V$ , as the space volume  
286 increases.

287 Equation 1 assumes a steady-state concentration of the virus has been  
288 reached based on the assumption that the exposure time,  $T$ , is significant.  
289 However, the time taken to reach the steady-state concentration in large  
290 spaces may be significant and affects the dose over shorter exposure periods.  
291 This is an example of the *reservoir effect*, the ability of indoor air to act as  
292 a fresh-air reservoir and absorb the impact of contaminant emissions. The  
293 greater the space volume, the greater the effect. These factors highlight the  
294 benefits of increasing the *per capita* space volume.

### 295 2.5. Exposure Time

296 Increasing exposure time when an infected person is present in the space  
297 for a significant period of time the exponent of Equation 1 becomes relatively  
298 small so that  $e^{-\phi T} \rightarrow 0$  and the inhaled dose is approximately proportional  
299 to the exposure time, however, the effect of the dose curve relationship means  
300 that *PPI* is not directly proportional to exposure time. Reducing the expo-  
301 sure time from 12 to 4 hours will reduce the probability of an inhaled dose  
302 leading to infection from relatively low viral load infectors, but will have less  
303 effect on the higher viral load infectors. It is only when exposure times be-  
304 come very short that the *PPI* reduces rapidly due to the reduced probability

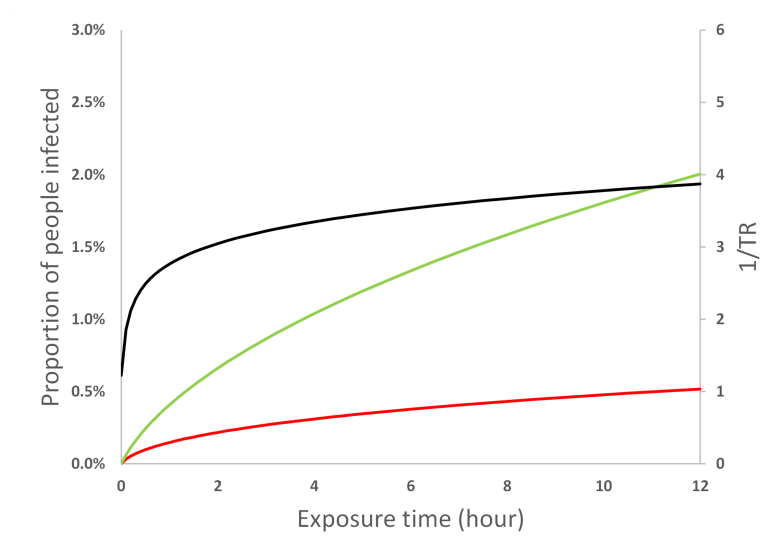


Figure 5: The effect of increasing the exposure time on the Big Office  $PPI$  (green), Small Office  $PPI$  (red) and the  $TR$  (black). As the exposure time increases, the dose increases, resulting in an increase in  $PPI$ . All values are illustrative.

305 of even the higher viral load infectors delivering a dose likely to lead to infec-  
 306 tion, (as this study assumes steady state, this rate of reduction will be more  
 307 pronounced when considering the reservoir effect) this is consistent with the  
 308 findings of Miller *et al.* in the requirement for reduced exposure time, as well  
 309 as improved ventilation to significantly reduce the risk of transmission in the  
 310 case of the Skagit choir superspreading event [14].

### 311 **3. Rapid Antigen Testing**

312 Lateral flow testing uses a rapid lateral flow device (LFD) based on col-  
 313 loidal gold immunochromatography designed to detect the presence of SARS-  
 314 CoV-2 nucleocapsid antigens in nasopharyngeal swabs. These tests are not  
 315 as sensitive as PCR tests in detecting the presence of SARS-CoV-2, but they  
 316 have been demonstrated to have a good ability at detecting higher viral loads

317 in infectors [36, 37]. Because the results of our analysis demonstrates that  
318 the higher viral emissions are responsible for the greater *PPI* we consider  
319 the effect of a scenario where widespread adoption of LFD use is success-  
320 ful in identifying individuals with high viral load and removing them from  
321 the scenario. The distribution of viral loads of infectors is assumed to be  
322 log normally distributed with a mean of  $\mu = 2.1 \times 10^9$  and a standard devi-  
323 ation of  $\sigma = 2.0 \times 10^{10}$ , then the proportion of individuals with viral loads  
324 greater than  $10^9$  RNA copies per ml is about 9%. We can assume a propor-  
325 tion of these are removed from the Small Office and Big Office scenarios and  
326 consider the effects on the *PPI* given the assumptions in Table 2. The prob-  
327 ability of viral load,  $P(L)$  when  $VL > 10^9$  RNA copies/ml is multiplied by  
328  $1 - LFD_{effectiveness}$  where the effectiveness is assumed to be 70%, Figure 6.  
329 These results show that LFD could be an effective measure to reduce the  
330 *PPI*, reducing both the absolute *PPI* in Big Office (from 1.59 to 0.60) and  
331 Small Office (from 0.43 to 0.22), as well as the *TR*. However, with a *C* of  
332 1 : 100, persons with a viral load greater than  $10^9$  RNA copies/ml represent  
333 around 0.09% of the total population, so although LFD could be an effective  
334 method of removing the highest viral loads from a scenario, a lot of lateral  
335 flow tests need to be conducted to capture every high viral load infector.

#### 336 **4. Alternative assumptions, lower virion viability and higher mode** 337 **viral load**

338 As detailed previously, the assumptions used in the main paper with  
339 respect to how RNA copies represent viable virions is highly conservative,  
340 and so below we use a more realistic value of 1% RNA copies as representing

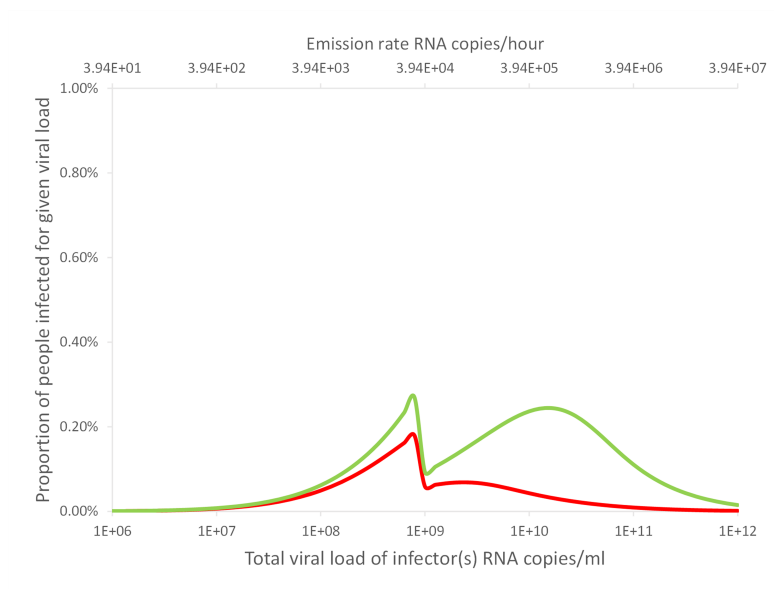


Figure 6: An indication of the relationship between the proportion of a population infected for a particular viral load when the community infection rate is  $C = 1\%$  and where LFD that are 70% effective at removing infectors with viral loads greater than  $10^9$  RNA copies per ml. The area under the curve represents the total proportion of people infected for the Small Office (red) and the Big Office (green). All values are illustrative.

341 viable virions. Additionally we also consider that the mode value for viral  
342 load is  $10^8$  RNA copies per ml, to represent a potential increase in viral load  
343 that could be the result of a variant of SARS-CoV-2, see Tables 4 and 5.

344 Figure 7 shows how the reduction in virion viability shifts the Big Office  
345 and Small Office dose curves to the right of the graph as greater viral emission  
346 is required to result in a dose of viable virion likely to give rise to an infection.  
347 The viral load and the probability that a single has that viral load,  $P(L)$ ,  
348 is also shifted to the right. The dashed vertical lines show the viral load  
349 required to give a 50% probability that the dose will lead to an infection for  
350 each scenario,  $P(R) = 50\%$ . The area under the blue curve to the right of  
351 each vertical line is the probability that the viral load of the infected person  
352 leads to  $P(R) \geq 50\%$ . The probability is much smaller for the Big Office,  
353 which has the lower REI. This probability that an infected person has a viral  
354 load that leads to  $P(R) \geq 50\%$  is small, suggesting that the most likely  
355 outcome is  $P(R) \leq 50\%$ .

356 The effect of varying assumptions on the shape of the plotted  $PPI$  curves  
357 have been described in detail in the main paper and above 2. In Figures 8  
358 and 9 the affect on  $PPI$  and  $TR$  is shown for the assumptions made in the  
359 main paper (on the left) with the higher modal viral load and lower virion  
360 viability (on the right). The effect on the absolute values is pronounced due  
361 to the reduced virion viability assumption, and given these assumptions the  
362  $PPI$  is very low, suggesting that far field transmission is likely to be rare and  
363 efforts taken to minimise  $TR$  should consider the absolute improvements in  
364  $PPI$  when assessing the benefits in  $TR$  reduction compared to the costs of,  
365 for example, the increased energy use needed to increase ventilation above

366 current guidance. It is important to note how changes in assumptions needed  
 367 to estimate viral emission rates have large impacts on absolute values of  $PPI$   
 368 and thus the uncertainty in these assumptions needs to be considered when  
 369 interpreting comparisons.

Table 4: Scenario inputs and calculations of individual risk.

	Big Office Reference	Small Office Comparator
Number of occupants, $N$	50	5
Space Volume, $V$ ( $\text{m}^3$ )	1500	150
<i>Per capita</i> volume, $V N^{-1}$ ( $\text{m}^3$ per person)	30	30
Air flow rate, $\psi V$ ( $\text{ls}^{-1}$ )	500	50
Air change rate, $\psi$ ( $\text{h}^{-1}$ )	1.2	1.2
Removal rate, $\phi$ ( $\text{h}^{-1}$ )	2.26	2.26
Equivalent ventilation rate, $\phi V$ ( $\text{ls}^{-1}$ )	942	94.2
Exposure time, $T$ (h)	8	8
Dose constant, $k$ [32]	410	410
Viable fraction, $v$ (%)	<b>1</b>	<b>1</b>
Viral load (RNA copies per ml) [35]	<b><math>10^8</math></b>	<b><math>10^8</math></b>
Respiratory activity, <i>breathing: talking</i> (%)	75:25	75:25
Viral emission rate, $G$ (RNA copies per hour)	394	394
Respiratory rate, $q_{sus}$ ( $\text{m}^3\text{h}^{-1}$ )	0.56	0.56
Community infection rate, $C$	1:100	1:100
Dose, $D$ (viable virions inhaled)	<b>0.002</b>	<b>0.025</b>
REI	1	10

All values converted to SI units before application.

370 For this analysis we make the assumption that 1% of genome copies  
 371 (RNA copies) represent viable virions, which is a more realistic magnitude to  
 372 assume given the literature

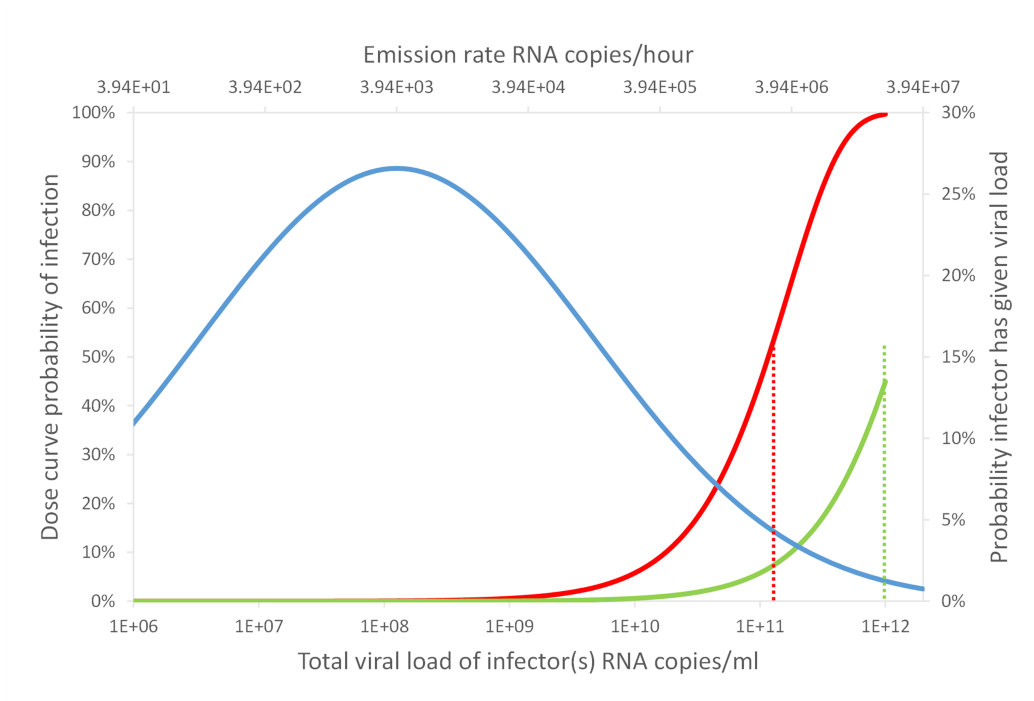


Figure 7: An indication of the relationship between the viral load,  $L$ , and the consequent probability of infection,  $P(R)$ , in the Big Office (green) and Small Office (red) for a susceptible occupant, and the probability of a single infected person having a viral load,  $P(L)$ , (blue). Dashed vertical lines indicate the viral load required for  $P(R) = 50\%$ .

Table 5: Scenario inputs and calculations of population risk.

	Big Office Reference	Small Office Comparator
Viral load [35] (RNA copies per ml)	<b>LN</b> ( $2.7 \times 10^{10}, 3.6 \times 10^{11}$ )	
$P(R)$ (%)	0.062	0.620
$P(I = 0)$ (%)	61	95
$P(0 < I < N)$ (%)	39	5
$\bar{I}$	1.27	1.02
$P(S)$ (%)	39	5
$PPI$ (%)	<b>0.241</b>	<b>0.119</b>
$TR$		0.49

LN, log-normal( $\mu, \sigma$ )  
All values converted to SI units before application.



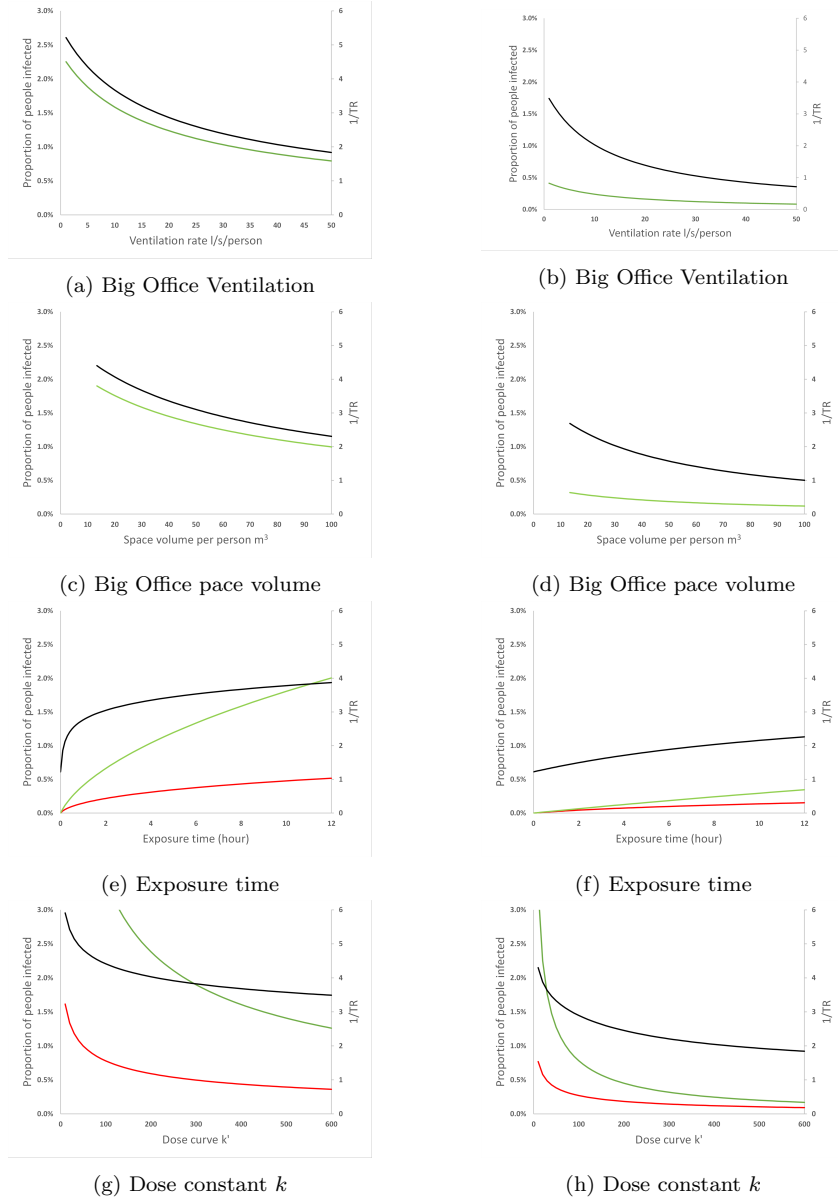


Figure 8: The effect of modulating assumption values on the Big Office *PPI* (green), Small Office *PPI* (red) and the *TR* (black). Left hand images the modal viral load assumed to be  $10^7$  RNA copies per ml and virion viability 100%, right hand images the modal viral load assumed to be  $10^8$  RNA copies per ml and virion viability 1%. All values are illustrative.

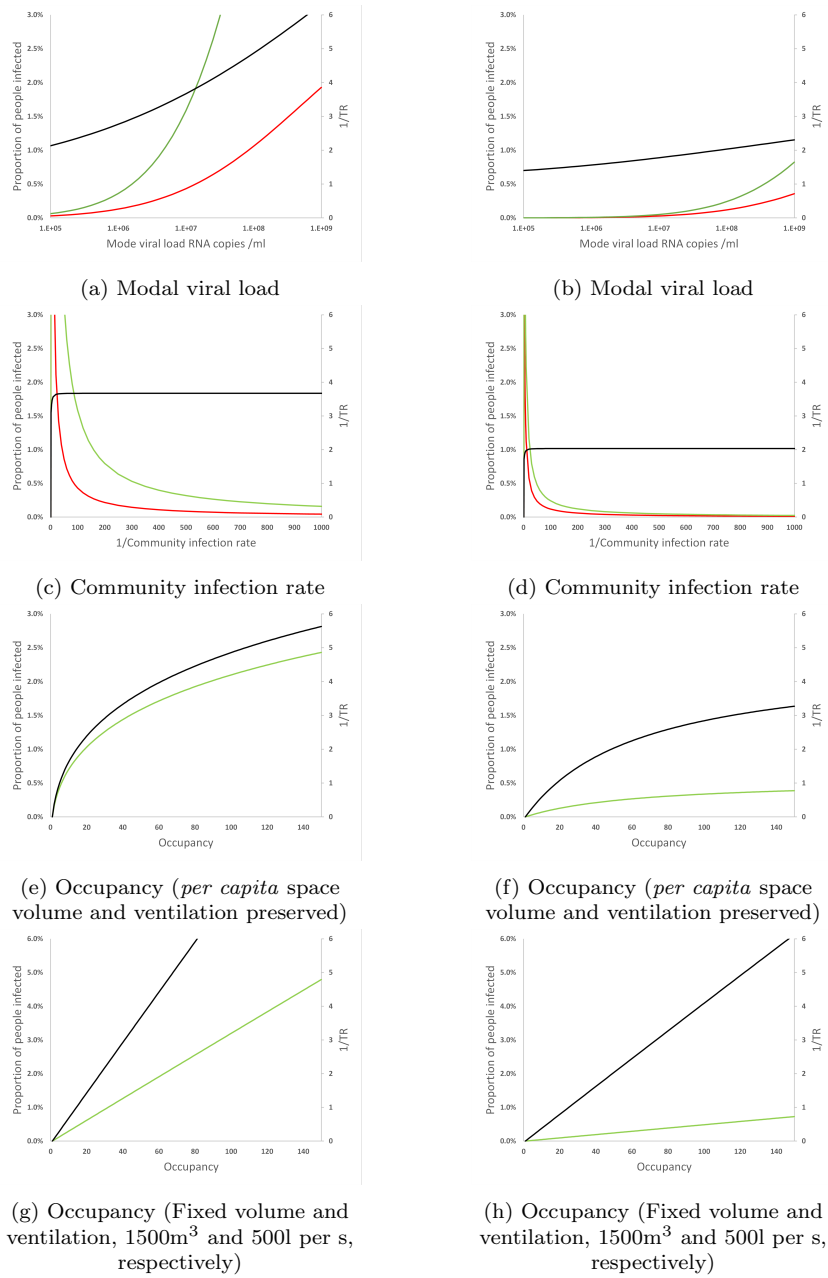


Figure 9: The effect of modulating assumption values on the Big Office *PPI* (green), Small Office *PPI* (red) and the *TR* (black). Left hand images the modal viral load assumed to be  $10^7$  RNA copies per ml and virion viability 100%, right hand images the modal viral load assumed to be  $10^8$  RNA copies per ml and virion viability 1%. All values are illustrative.

373 **5. Equations**

374 See main text for explanations of the equations.

375 *5.1. Inhaled Dose*

$$D \simeq \frac{K q_{sus} G T v}{\phi V} \quad (1)$$

376 *5.2. Dose response curve*

$$P(R) = 1 - e^{-D/k} \quad (2)$$

377 **Acknowledgements**

378 The authors acknowledge the Engineering and Physical Sciences Research  
379 Council (EP/W002779/1) who financially supported this work. They are also  
380 grateful to Constanza Molina for her comments on this paper.

381 **References**

- 382 [1] T. Watanabe, T. A. Bartrand, M. H. Weir, T. Omura, C. N. Haas,  
383 Development of a dose-response model for sars coronavirus. risk analysis:  
384 an official publication of the society for risk analysis, Risk Anal 30 (7)  
385 (2010) 1129–1138. doi:10.1111/j.1539-6924.2010.01427.x.
- 386 [2] H. Parhizkar, K. G. Van Den Wymelenberg, C. N. Haas, R. L. Corsi, A  
387 Quantitative Risk Estimation Platform for Indoor Aerosol Transmission of  
388 COVID-19, Risk Analysis 0 (0) (2021). doi:10.1111/risa.13844.
- 389 [3] X. Zhang, J. Wang, Dose-response Relation Deduced for Coronaviruses  
390 From Coronavirus Disease 2019, Severe Acute Respiratory Syndrome,  
391 and Middle East Respiratory Syndrome: Meta-analysis Results and  
392 its Application for Infection Risk Assessment of Aerosol Transmission,  
393 Clinical Infectious Diseases (Xx Xxxx) (2020) 1–5. doi:10.1093/cid/  
394 ciaa1675.
- 395 [4] J. Schijven, L. C. Vermeulen, A. Swart, A. Meijer, E. Duizer, A. M.  
396 de Roda Husman, Quantitative microbial risk assessment for airborne  
397 transmission of sars-cov-2 via breathing, speaking, singing, coughing,  
398 and sneezing, Environmental Health Perspectives 129 (4) (2021) 1–10.  
399 doi:10.1289/EHP7886.
- 400 [5] M. Cevik, K. Kuppalli, J. Kindrachuk, M. Peiris, Virology, transmission,  
401 and pathogenesis of SARS-CoV-2, The BMJ 371 (2020) 1–6. doi:10.  
402 1136/bmj.m3862.

- 403 [6] M. Cevik, M. Tate, O. Lloyd, A. E. Maraolo, J. Schafers, A. Ho,  
404 SARS-CoV-2, SARS-CoV, and MERS-CoV viral load dynamics, du-  
405 ration of viral shedding, and infectiousness: a systematic review and  
406 meta-analysis, *The Lancet Microbe* 2 (1) (2021) e13–e22. doi:10.1016/  
407 S2666-5247(20)30172-5.  
408 URL [http://dx.doi.org/10.1016/S2666-5247\(20\)30172-5](http://dx.doi.org/10.1016/S2666-5247(20)30172-5)
- 409 [7] Y. Pan, D. Zhang, P. Yang, L. L. Poon, Q. Wang, Viral load of SARS-  
410 CoV-2 in clinical samples, *The Lancet Infectious Diseases* 20 (4) (2020)  
411 411–412. doi:10.1016/S1473-3099(20)30113-4.  
412 URL [http://dx.doi.org/10.1016/S1473-3099\(20\)30113-4](http://dx.doi.org/10.1016/S1473-3099(20)30113-4)
- 413 [8] S. Karimzadeh, R. Bhopal, H. Nguyen Tien, Review of infective  
414 dose, routes of transmission and outcome of COVID-19 caused  
415 by the SARS-COV-2: comparison with other respiratory viruses–  
416 CORRIGENDUM, *Epidemiology and Infection* 149 (2021) e116.  
417 doi:10.1017/S0950268821001084.  
418 URL [https://www.cambridge.org/core/product/identifier/  
419 S0950268821001084/type/journal\\_article](https://www.cambridge.org/core/product/identifier/S0950268821001084/type/journal_article)
- 420 [9] R. Challen, E. Brooks-Pollock, J. M. Read, L. Dyson, K. Tsaneva-  
421 Atanasova, L. Danon, Risk of mortality in patients infected with SARS-  
422 CoV-2 variant of concern 202012/1: Matched cohort study, *The BMJ*  
423 372 (2021) 1–10. doi:10.1136/bmj.n579.
- 424 [10] R. Ke, P. P. Martinez, R. L. Smith, L. L. Gibson, A. Mirza, M. Conte,  
425 N. Gallagher, C. H. Luo, J. Jarrett, A. Conte, M. Farjo, K. K. O.  
426 Walden, G. Rendon, C. J. Fields, R. Fredrickson, D. C. Edmonson,

- 427 M. E. Baughman, K. K. Chiu, J. Yedetore, J. Quicksall, A. N. Owens,  
428 J. Broach, Daily sampling of early SARS-CoV-2 infection reveals  
429 substantial heterogeneity in infectiousness, medRxiv (July 12th 2021)  
430 (2021) 1–23. doi:<https://doi.org/10.1101/2021.07.12.21260208>.  
431 URL [https://www.medrxiv.org/content/10.1101/2021.07.12.](https://www.medrxiv.org/content/10.1101/2021.07.12.21260208v1)  
432 [21260208v1](https://www.medrxiv.org/content/10.1101/2021.07.12.21260208v1)
- 433 [11] A. S. Walker, E. Pritchard, T. House, J. V. Robotham, P. J. Birrell,  
434 I. Bell, J. Bell, J. Newton, J. Farrar, I. Diamond, R. Studley, J. Hay,  
435 K.-D. Vihta, T. E. Peto, N. Stoesser, P. C. Matthews, D. W. Eyre,  
436 K. Pouwels, Ct threshold values, a proxy for viral load in community  
437 SARS-CoV-2 cases, demonstrate wide variation across populations and  
438 over time, eLife 10 (jul 2021). doi:[10.7554/eLife.64683](https://doi.org/10.7554/eLife.64683).  
439 URL <https://elifesciences.org/articles/64683>
- 440 [12] P. Z. Chen, N. Bobrovitz, Z. Premji, M. Koopmans, D. N. Fisman, F. X.  
441 Gu, Heterogeneity in transmissibility and shedding SARS-CoV-2 via  
442 droplets and aerosols, eLife 10 (2021) 1–32. doi:[10.7554/eliflife.65774](https://doi.org/10.7554/eliflife.65774).
- 443 [13] G. Buonanno, L. Stabile, L. Morawska, Estimation of airborne viral  
444 emission: Quanta emission rate of SARS-CoV-2 for infection risk as-  
445 sessment, Environment International 141 (May) (2020) 105794. doi:  
446 [10.1016/j.envint.2020.105794](https://doi.org/10.1016/j.envint.2020.105794).
- 447 [14] S. L. Miller, W. W. Nazaroff, J. L. Jimenez, A. Boerstra, S. J. Dancer,  
448 J. Kurnitski, L. C. Marr, L. Morawska, C. Noakes, Transmission of  
449 SARS-CoV-2 by inhalation of respiratory aerosol in the Skagit Valley

- 450 Chorale superspreading event, *Indoor Air* in press (2020). doi:doi.  
451 org/10.1111/ina.12751.
- 452 [15] J. Yan, M. Grantham, J. Pantelic, P. J. B. De Mesquita, B. Albert,  
453 F. Liu, S. Ehrman, D. K. Milton, Infectious virus in exhaled breath of  
454 symptomatic seasonal influenza cases from a college community, *Pro-*  
455 *ceedings of the National Academy of Sciences of the United States of*  
456 *America* 115 (5) (2018) 1081–1086. doi:10.1073/pnas.1716561115.
- 457 [16] Q. Yang, T. K. Saldi, P. K. Gonzales, E. Lasda, C. J. Decker, K. L.  
458 Tat, M. R. Fink, C. R. Hager, J. C. Davis, C. D. Ozeroff, D. Muhrad,  
459 S. K. Clark, W. T. Fattor, N. R. Meyerson, C. L. Paige, A. R. Gilchrist,  
460 A. Barbachano-Guerrero, E. R. Worden-Sapper, S. S. Wu, G. R. Bris-  
461 son, M. B. McQueen, R. D. Dowell, L. Leinwand, R. Parker, S. L.  
462 Sawyer, Just 2 percent of sars-cov-2 positive individuals carry 90 per-  
463 cent of the virus circulating in communities, *Proceedings of the National*  
464 *Academy of Sciences* 118 (21) (2021) e2104547118. doi:10.1073/pnas.  
465 2104547118.  
466 URL <http://www.pnas.org/lookup/doi/10.1073/pnas.2104547118>
- 467 [17] D. K. Milton, M. P. Fabian, B. J. Cowling, M. L. Grantham, J. J.  
468 McDevitt, Influenza Virus Aerosols in Human Exhaled Breath: Particle  
469 Size, Culturability, and Effect of Surgical Masks, *PLoS Pathogens* 9 (3)  
470 (2013). doi:10.1371/journal.ppat.1003205.
- 471 [18] P. Fabian, J. J. McDevitt, W. H. DeHaan, R. O. Fung, B. J. Cowling,  
472 K. H. Chan, G. M. Leung, D. K. Milton, Influenza virus in human

- 473 exhaled breath: An observational study, PLoS ONE 3 (7) (2008) 5–10.  
474 doi:10.1371/journal.pone.0002691.
- 475 [19] K. K. Coleman, D. J. W. Tay, K. S. Tan, S. W. X. Ong, T. S. Than,  
476 M. H. Koh, Y. Q. Chin, H. Nasir, T. M. Mak, J. J. H. Chu, D. K. Milton,  
477 V. T. K. Chow, P. A. Tambyah, M. Chen, K. W. Tham, Viral Load of  
478 Severe Acute Respiratory Syndrome Coronavirus 2 (SARS-CoV-2) in  
479 Respiratory Aerosols Emitted by Patients With Coronavirus Disease  
480 2019 (COVID-19) While Breathing, Talking, and Singing, Clinical  
481 Infectious Diseases 2 (Xx) (2021) 1–7. doi:10.1093/cid/ciab691.  
482 URL [https://academic.oup.com/cid/advance-article/doi/10.](https://academic.oup.com/cid/advance-article/doi/10.1093/cid/ciab691/6343417)  
483 [1093/cid/ciab691/6343417](https://academic.oup.com/cid/advance-article/doi/10.1093/cid/ciab691/6343417)
- 484 [20] F. K. Gregson, N. A. Watson, C. M. Orton, A. E. Haddrell, L. P. Mc-  
485 Carthy, T. J. Finnie, N. Gent, G. C. Donaldson, P. L. Shah, J. D.  
486 Calder, B. R. Bzdek, D. Costello, J. P. Reid, Comparing aerosol concen-  
487 trations and particle size distributions generated by singing, speaking  
488 and breathing, Aerosol Science and Technology 55 (6) (2021) 681–691.  
489 doi:10.1080/02786826.2021.1883544.  
490 URL <https://doi.org/10.1080/02786826.2021.1883544>
- 491 [21] G. R. Johnson, L. Morawska, The mechanism of breath aerosol forma-  
492 tion, Journal of Aerosol Medicine and Pulmonary Drug Delivery 22 (3)  
493 (2009) 229–237. doi:10.1089/jamp.2008.0720.
- 494 [22] G. R. Johnson, L. Morawska, Z. D. Ristovski, M. Hargreaves,  
495 K. Mengersen, C. Y. Chao, M. P. Wan, Y. Li, X. Xie, D. Kato-  
496 shevski, S. Corbett, Modality of human expired aerosol size distri-



- 497 butions, *Journal of Aerosol Science* 42 (12) (2011) 839–851. doi:  
498 10.1016/j.jaerosci.2011.07.009.
- 499 [23] L. Morawska, G. R. Johnson, Z. D. Ristovski, M. Hargreaves,  
500 K. Mengersen, S. Corbett, C. Y. Chao, Y. Li, D. Katoshevski, Size  
501 distribution and sites of origin of droplets expelled from the human res-  
502 piratory tract during expiratory activities, *Journal of Aerosol Science*  
503 40 (3) (2009) 256–269. doi:10.1016/j.jaerosci.2008.11.002.
- 504 [24] O. O. Adenaiye, J. Lai, P. J. B. de Mesquita, F. Hong, S. Youssefi,  
505 J. German, S.-H. S. Tai, B. Albert, M. Schanz, S. Weston, J. Hang,  
506 C. Fung, H. K. Chung, K. K. Coleman, N. Sapoval, T. Treangen,  
507 I. M. Berry, K. Mullins, M. Frieman, T. Ma, D. K. Milton, Infec-  
508 tious SARS-CoV-2 in Exhaled Aerosols and Efficacy of Masks Dur-  
509 ing Early Mild Infection, medRxiv (2021) 1–19arXiv:2021.08.13.  
510 21261989, doi:<https://doi.org/10.1101/2021.08.13.21261989>.  
511 URL <https://doi.org/10.1101/2021.08.13.21261989>
- 512 [25] G. Buonanno, L. Morawska, L. Stabile, Quantitative assessment of the  
513 risk of airborne transmission of SARS-CoV-2 infection: Prospective and  
514 retrospective applications, *Environment International* 145 (June) (2020)  
515 106112. doi:10.1016/j.envint.2020.106112.  
516 URL <https://doi.org/10.1016/j.envint.2020.106112>
- 517 [26] A. C. Fears, W. B. Klimstra, P. Duprex, A. Hartman, S. C. Weaver,  
518 K. S. Plante, D. Mirchandani, J. A. Plante, P. V. Aguilar, D. Fernández,  
519 A. Nalca, A. Totura, D. Dyer, B. Kearney, M. Lackemeyer, J. K. Bo-  
520 hannon, R. Johnson, R. F. Garry, D. S. Reed, C. J. Roy, Persistence

- 521 of Severe Acute Respiratory Syndrome Coronavirus 2 in Aerosol Sus-  
522 pensions, *Emerging infectious diseases* 26 (9) (2020). doi:10.3201/  
523 eid2609.201806.
- 524 [27] B. Jones, P. Sharpe, C. Iddon, E. A. Hathway, C. J. Noakes, S. Fitzger-  
525 ald, Modelling uncertainty in the relative risk of exposure to the SARS-  
526 CoV-2 virus by airborne aerosol transmission in well mixed indoor air,  
527 *Building and Environment* 191 (October 2020) (2021) 107617. doi:  
528 10.1016/j.buildenv.2021.107617.  
529 URL <https://doi.org/10.1016/j.buildenv.2021.107617>
- 530 [28] J. Lelieveld, F. Helleis, S. Borrmann, Y. Cheng, F. Drewnick, G. Haug,  
531 T. Klimach, J. Sciare, H. Su, U. Pöschl, Model calculations of aerosol  
532 transmission and infection risk of covid-19 in indoor environments, *Inter-  
533 national Journal of Environmental Research and Public Health* 17 (21)  
534 (2020) 1–18. doi:10.3390/ijerph17218114.
- 535 [29] P. Y. Chia, K. K. Coleman, Y. K. Tan, S. Wei, X. Ong, M. Gum, S. K.  
536 Lau, X. F. Lim, A. S. Lim, S. Sutjipto, P. H. Lee, T. T. Son, B. E. Young,  
537 D. K. Milton, G. C. Gray, S. Schuster, T. Barkham, P. P. De, S. Vasoo,  
538 M. Chan, B. Sze, P. Ang, Detection of air and surface contamination by  
539 SARS-CoV-2 in hospital rooms of infected patients, *Nature Communi-  
540 cations* 11 (2800) (2020). doi:10.1038/s41467-020-16670-2.
- 541 [30] J. Ma, X. Qi, H. Chen, X. Li, Z. Zhang, H. Wang, L. Sun, L. Zhang,  
542 J. Guo, L. Morawska, S. A. Grinshpun, P. Biswas, R. C. Flagan, M. Yao,  
543 Coronavirus Disease 2019 Patients in Earlier Stages Exhaled Millions of

- 544 Severe Acute Respiratory Syndrome Coronavirus 2 Per Hour, *Clinical in-*  
545 *fectious diseases : an official publication of the Infectious Diseases Soci-*  
546 *ety of America* 72 (10) (2021) e652–e654. doi:10.1093/cid/ciaa1283.
- 547 [31] V. M. Corman, I. Eckerle, T. Bleicker, A. Zaki, O. Landt, M. Eschbach-  
548 Bludau, S. van Boheemen, R. Gopal, M. Ballhause, T. M. Bestebroer,  
549 D. Muth, M. A. Müller, J. F. Drexler, M. Zambon, A. D. Osterhaus,  
550 R. M. Fouchier, C. Drosten, Detection of a novel human coronavirus by  
551 real-time reverse-transcription polymerase chain reaction, *Eurosurveil-*  
552 *lance* 17 (39) (2012) 1–6. doi:10.2807/ese.17.39.20285-en.  
553 URL <http://dx.doi.org/10.2807/ese.17.39.20285-en>
- 554 [32] M. L. DeDiego, L. Pewe, E. Alvarez, M. T. Rejas, S. Perlman, L. En-  
555 juanes, Pathogenicity of severe acute respiratory coronavirus deletion  
556 mutants in hACE2 transgenic mice, *Virology* 376 (2) (2008) 379–389.  
557 doi:<https://doi.org/10.1016/j.virol.2008.03.005>.  
558 URL [https://www.sciencedirect.com/science/article/pii/](https://www.sciencedirect.com/science/article/pii/S004268220800175X)  
559 [S004268220800175X](https://www.sciencedirect.com/science/article/pii/S004268220800175X)
- 560 [33] F. Aiano, A. A. Mensah, K. McOwat, C. Obi, A. Vusirikala, A. A.  
561 Powell, J. Flood, J. Bosowski, L. Letley, S. Jones, Z. Amin-Chowdhury,  
562 J. Lacy, I. Hayden, S. A. Ismail, M. E. Ramsay, S. N. Ladhani, V. Saliba,  
563 COVID-19 outbreaks following full reopening of primary and secondary  
564 schools in England: Cross-sectional national surveillance, November  
565 2020, *The Lancet Regional Health - Europe* 6 (May 2020) (2021) 100120.  
566 doi:10.1016/j.lanepe.2021.100120.
- 567 [34] ONS, ONS Coronavirus (COVID-19) Infection Survey.

- 568 URL [https://www.ons.gov.uk/peoplepopulationandcommunity/](https://www.ons.gov.uk/peoplepopulationandcommunity/healthandsocialcare/conditionsanddiseases/bulletins/coronaviruscovid19infectionsurveypilot/previousReleases)  
569 [healthandsocialcare/conditionsanddiseases/bulletins/](https://www.ons.gov.uk/peoplepopulationandcommunity/healthandsocialcare/conditionsanddiseases/bulletins/coronaviruscovid19infectionsurveypilot/previousReleases)  
570 [coronaviruscovid19infectionsurveypilot/previousReleases](https://www.ons.gov.uk/peoplepopulationandcommunity/healthandsocialcare/conditionsanddiseases/bulletins/coronaviruscovid19infectionsurveypilot/previousReleases)
- 571 [35] P. Z. Chen, N. Bobrovitz, Z. Premji, M. Koopmans, D. N. Fisman, F. X.  
572 Gu, Sars-cov-2 shedding dynamics across the respiratory tract, sex, and  
573 disease severity for adult and pediatric covid-19, *eLife* 10 (2021) e70458.  
574 doi:10.7554/eLife.70458.  
575 URL <https://doi.org/10.7554/eLife.70458>
- 576 [36] J. Ferguson, S. Dunn, A. Best, J. Mirza, B. Percival, M. Mayhew,  
577 O. Megram, F. Ashford, T. White, E. Moles-Garcia, L. Crawford,  
578 T. Plant, A. Bosworth, M. Kidd, A. Richter, J. Deeks, A. McNally,  
579 Validation testing to determine the sensitivity of lateral flow testing for  
580 asymptomatic SARSCoV-2 detection in low prevalence settings: Test-  
581 ing frequency and public health messaging is key, *PLoS Biology* 19 (4)  
582 (2021) 1–9. doi:10.1371/journal.pbio.3001216.  
583 URL <http://dx.doi.org/10.1371/journal.pbio.3001216>
- 584 [37] L. Y. W. Lee, S. Rozmanowski, M. Pang, A. Charlett, C. Anderson,  
585 G. J. Hughes, M. Barnard, L. Peto, R. Vipond, A. Sienkiewicz,  
586 S. Hopkins, J. Bell, D. W. Crook, N. Gent, A. S. Walker, T. E. A.  
587 Peto, D. W. Eyre, Severe Acute Respiratory Syndrome Coronavirus  
588 2 (SARS-CoV-2) Infectivity by Viral Load, S Gene Variants and  
589 Demographic Factors, and the Utility of Lateral Flow Devices to  
590 Prevent Transmission, *Clinical Infectious Diseases* 6 (2021) 1–32.  
591 doi:10.1093/cid/ciab421.

592 URL <https://academic.oup.com/cid/advance-article/doi/10.1093/cid/ciab421/6273394>